

pubs.acs.org/JACS Article

# Impact of Pt(hkl) Electrode Surface Structure on the Electrical Double Layer Capacitance

Song Xue, Payal Chaudhary, Mohammad Reza Nouri, Elena Gubanova, Batyr Garlyyev, Vitaly Alexandrov, and Aliaksandr S. Bandarenka\*



Cite This: https://doi.org/10.1021/jacs.3c11403



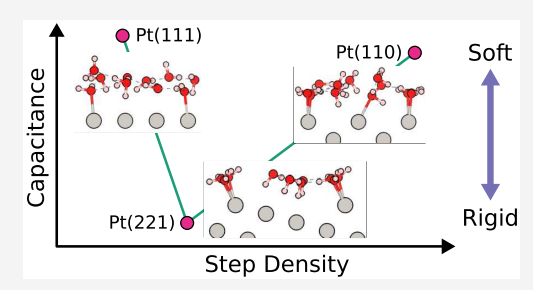
**ACCESS** I

III Metrics & More

Article Recommendations

Supporting Information

ABSTRACT: The classical theory of the electrical double layer (EDL) does not consider the effects of the electrode surface structure on the EDL properties. Moreover, the best agreement between the traditional EDL theory and experiments has been achieved so far only for a very limited number of ideal systems, such as liquid metal mercury electrodes, for which it is challenging to operate with specific surface structures. In the case of solid electrodes, the predictive power of classical theory is often not acceptable for electrochemical energy applications, e.g., in supercapacitors, due to the effects of surface structure, electrode composition, and complex electrolyte contributions. In this work, we combine *ab initio* molecular dynamics (AIMD) simulations and



electrochemical experiments to elucidate the relationship between the structure of Pt(hkl) surfaces and the double-layer capacitance as a key property of the EDL. Flat, stepped, and kinked Pt single crystal facets in contact with acidic  $HClO_4$  media are selected as our model systems. We demonstrate that introducing specific defects, such as steps, can substantially reduce the EDL capacitances close to the potential of zero charge (PZC). Our AIMD simulations reveal that different Pt facets are characterized by different net orientations of the water dipole moment at the interface. That allows us to rationalize the experimentally measured (inverse) volcano-shaped capacitance as a function of the surface step density.

#### INTRODUCTION

The properties of electrified interfaces between electron and ion conductors have been the focus of research since the 19th century. In the first half of the 20th century, the electrical double layer (EDL) theory was mainly established in its conventional form. 1-3 Recently, attempts have been undertaken to improve it, taking into account new experimental data and the results of theoretical research (see, e.g., refs 4-11), which critically question the overall predictive and explanatory power of the classical EDL theory. In contrast to the pillars of that theory, it is nowadays clear that the electrode structure, its composition, the nature of the electrolyte constituents, and some other aspects contribute to the properties of the EDL. However, an improved understanding of the EDL properties is essential to predicting the functionalities of electrochemical systems. For instance, it is necessary to maximize the EDL capacitances in supercapacitors or to normalize the electrocatalytic activity for energy conversion and storage devices. 12-16

Among other groups, we have recently reported that model Pt, Pd, Cu, and Au electrodes demonstrate a somewhat counterintuitive dependence of EDL capacitances on the structure of the electrode surface,  $^{17}$  its chemical nature, and the nature of the alkali metal cations present in the electrolyte. For example, we demonstrated that for both Pt(111) and Au(111) in 0.05 M AMClO<sub>4</sub> (AM = Li<sup>+</sup>, Na<sup>+</sup>, K<sup>+</sup>,

Rb<sup>+</sup>, Cs<sup>+</sup>), the EDL capacitance depends linearly on the hydration energy of the alkali metal cation, with the higher hydration energies corresponding to the lower EDL capacitances close to the potential of zero charge (PZC). <sup>18,19</sup> This finding cannot be straightforwardly explained by specific adsorption of the cations, as in this case, the trends should be the opposite of the radii of the cations increase. Such nontrivial dependencies of the key electrochemical properties, such as the EDL capacitance on the presumably inert electrolyte species, require more detailed mechanistic interpretations.

One of the basic parameters characterizing the properties of electrochemical interfaces is the electrode structure. It is known that different facets of the same metal electrode could exhibit drastically different electrocatalytic properties. However, the classical theory of the EDL completely ignores the role of the electrode surface structure, providing the best agreement with experiments only for a very limited number of ideal systems such as liquid metal mercury electrodes. <sup>1,20,21</sup> Pt is probably the most studied electrode material in electro-

Received: October 13, 2023 Revised: January 12, 2024 Accepted: January 16, 2024



catalysis owing to its superior properties, for example, to catalyze the hydrogen evolution reaction (HER). Nevertheless, even some basic electrochemical properties of Pt, such as the EDL capacitance, remain not well investigated. Exploring the EDL capacitance, particularly on different surface structures, will enable a better comparison across various electrocatalytic materials and fill gaps in traditional EDL theory.

In this work, we employ accurate impedance spectroscopy measurements to demonstrate on the example of Pt(hkl)single-crystal electrodes in acidic media that the EDL capacitance is highly sensitive to the electrode structure. To provide atomistic insights into the behavior of the EDL capacitances for a set of Pt surfaces and allow for explicit treatment of the Pt/water interfaces, we also undertake complementary ab initio molecular dynamics (AIMD) simulations.

## EXPERIMENTAL SECTION

**Electrochemical Experiments.** Prior to each experiment, the Pt crystals were prepared using a conventional flame annealing method. Bead-type Pt(111) (Icryst, Jülich, Germany), Pt(775), Pt(221) (provided by Prof. Juan Feliu, Alicante, Spain), Pt(12 10 5), Pt(331), and Pt(110) (obtained from Icryst, Jülich, Germany) electrodes were annealed by an isobutene flame and subsequently cooled in a mixture of 1000 ppm of CO (4.7, Air Liquide, Germany) in Ar (5.0, Air Liquide, Germany). Their cyclic voltammograms (CVs) were recorded in Ar-saturated 0.1 M HClO<sub>4</sub> (Suprapur, Merck, Germany) and used to ensure the surface structure quality by comparing with their respective "fingerprint" CVs.<sup>2</sup>

The electrochemical setup was cleaned using freshly prepared peroxymonosulfuric acid (7:3 ratios of H<sub>2</sub>SO<sub>4</sub> and H<sub>2</sub>O<sub>2</sub>). After the cleaning, the setup was rinsed several times with boiling ultrapure water. The setup consisted of three electrodes, including a mercury/ mercury-sulfate electrode (MMS) (SI Analytics, Germany) and a platinum wire (99.99%, Goodfellow, Germany), serving as the reference and counter electrodes, respectively. For details on the electrochemical setup and cleaning procedures, please refer to ref 22.

The electrochemical impedance spectroscopy (EIS) measurements were performed in the ac-frequency range of 30 kHz to 1 Hz. Note that a shunt capacitor ( $\sim$ 4  $\mu$ F) was added between the reference and counter electrodes to address the artifacts caused by the potentiostat at higher frequencies. The obtained impedance spectra were analyzed by the EIS Spectrum Analyzer 1.3 software 23 using an equivalent electric circuit that included the constant phase element (CPE) to describe the double-layer response. The root-mean-square deviations and individual parameter uncertainties ensured the modeling and fitting quality in the EIS data analysis. The exponent n obtained from fitting the equation  $Z_{DL} = C_{DL}^{\prime -1} \cdot (j\omega)^{-n}$  for the CPE remained consistently higher than 0.9, suggesting that the parameter  $C'_{DL}$  is close to the true EDL capacitance. It should be additionally noted that the exponent is very close to 1 at the double layer capacitance minima. Note that all of the EIS measurements were conducted close to the regions where no significant Faradaic reactions occurred, as shown in the corresponding CVs (Figure 1). Additionally, the fitted EIS curves matched the experimental curves well.

All electrochemical measurements were performed by using a VSP-300 potentiostat (Bio-Logic, France). All potentials used in this study were referred to the reversible hydrogen electrode (RHE). Parametrization of the Pt(hkl) surfaces was done using the generalized coordination number (GCN)<sup>24,25</sup> approach (see Supporting Information (SI), Figure S1), similar to our previous study.

Computational Details. Ab initio molecular dynamics (AIMD) simulations were conducted using the CP2K package.<sup>2</sup> electronic orbitals of Pt, O, and H atoms were described by using DZVP-MOLOPT-SR-GTH basis functions. The Goedecker-Teter-Hutter (GTH) pseudopotentials<sup>27</sup> with 18 valence electrons for Pt, 6 valence electrons for O, and 1 valence electron for H were employed. The Perdew-Burke-Ernzerhof (PBE) exchange-correlation func-

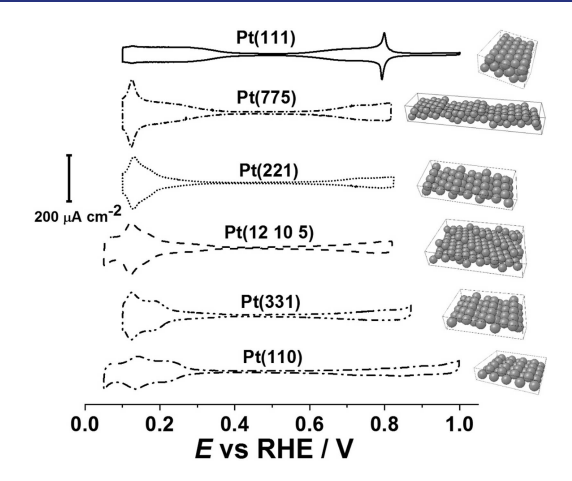


Figure 1. Typical cyclic voltammograms of Pt(hkl) electrodes recorded in Ar-saturated 0.1 M HClO<sub>4</sub>. Scan rate: 50 mV/s.

tional<sup>28</sup> was utilized. The plane wave basis set cutoff energy was set to 400 Ry to ensure accurate results. To account for the van der Waals dispersion forces, the DFT-D3 method of Grimme<sup>29,30</sup> was employed in all simulations. The Pt atoms were kept fixed in all of the AIMD simulations.

Water molecules were inserted into the vacuum gap of about 22 Å to achieve a total water density of  $\sim 1$  g/cm<sup>3</sup>. The thickness of the vacuum gap was chosen to have roughly 7-8 layers of water molecules between the opposite Pt surfaces. Figure S2 shows the water density distribution as a function of the distance from the Pt electrode surface, demonstrating that the water region is thick enough to reach the density of bulk water in the middle of the gap. Figure S3 shows the atomic structures of all four constructed periodic slabs, while the corresponding dimensions are listed in Table S1. For our computations, we chose to consider only four representative Pt facets with the following step densities: 0 nm<sup>-1</sup> for Pt (111), 1.19 nm<sup>-1</sup> for Pt (221), 1.63 nm<sup>-1</sup> for Pt (331), and 2.51 nm<sup>-1</sup> for Pt (110). For the analysis of AIMD trajectories, we chose the first two water layers by averaging over both sides of the slab. The distance from the electrode surface (z coordinate) for the nonzero step density facets, i.e., for Pt (221), Pt (331), and Pt (110), is taken as the midpoint between the outermost and innermost Pt atoms of the step. It can be seen from Figure S2 that the thickness of the first two water layers is in the range 1.5-2.2 Å and thus should provide a major contribution to the EDL capacitance, which is taken for our analysis.

The AIMD equilibration process involved 20 ps of NVT simulations at 330 K followed by 1 ps of NVE equilibration and 15 ps of NVE production runs. A time step of 0.5 fs was applied, and the mass of H was set to 3 amu. Our test calculations demonstrated no significant difference between the results with the H mass of 1 and 3 amu (see SI). We also compared the results of a shorter 9 ps production run with a total trajectory of 15 ps, revealing no significant qualitative changes (see SI). In the subsequent analysis of AIMD trajectories, we considered the coordinates at every 50 MD steps. While plotting distributions, the positions of water molecules were determined by the positions of the O atoms (see SI). An alternative to this is to consider the center of mass. However, the center of mass is already close to the O atom due to the small mass of H, and therefore approximating the position of O as the position of the water molecule serves as a good approximation. The time evolution of average temperatures during the NVE runs for each Pt/water system are shown in Figure S4.

#### RESULTS AND DISCUSSION

To investigate the relations between the EDL capacitance and electrode surface structure, we measured the  $C'_{DL}$  for flat, stepped, and kinked Pt single crystal facets, i.e., Pt(111), Pt(775), Pt(221), Pt(12 10 5), Pt(331), and Pt(110) surfaces

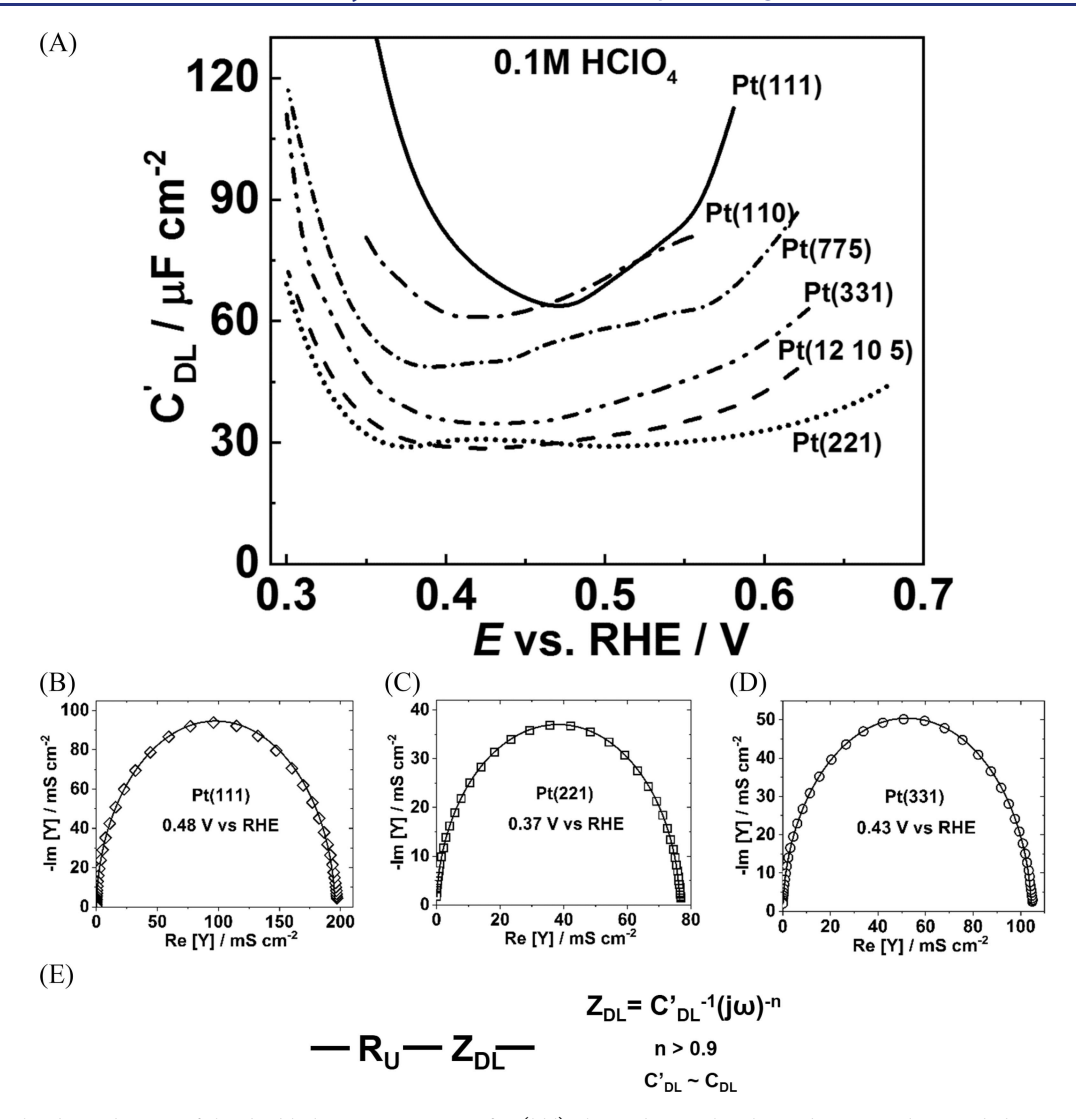


Figure 2. (A) The dependencies of the double layer capacitance of Pt(hkl) electrodes on the electrode potentials recorded in Ar-saturated 0.1 M  $HClO_4$  with (B-D) examples of the impedance spectra with fitting (solid lines). (E) The equivalent electric circuit was used for the fitting of the impedance spectra.

under the same conditions. Before each EIS measurement, the surface quality was checked by cyclic voltammetry in Arsaturated 0.1 M HClO<sub>4</sub>. As depicted in Figure 1, the CV obtained on the flat facets can be divided into three regions—the adsorption/desorption of hydroxide species (OH<sub>ads/des</sub>), the double layer region, and the adsorption/desorption of hydrogen (H<sub>ads/des</sub>)—whereas for CVs on the stepped and kinked facets, the emerging peaks observed at ~0.15 V versus RHE are assigned to the exchange between adsorbed hydrogen and hydroxyl along the step sites. As different surface structures can lead to varied behaviors of both H<sub>ads/des</sub> and OH<sub>ads/des</sub>, the CV shape of a Pt single crystal can indicate its surface structure quality. The obtained CVs are identical with those in the literature and confirm the presence of the surfaces in Figure 1.

 $C_{DL}^{\prime}$  dependencies for the Pt(hkl) electrodes were measured in 0.1 M HClO<sub>4</sub> (Figure 2). As mentioned earlier, EIS measurements were conducted close to the regions where no significant Faradaic reactions occurred, as shown in the corresponding CVs. The EIS spectra were fitted by an equivalent electric circuit shown in Figure 2E, in which the CPE was used to describe the double-layer response. The fitted

EIS curves matched the experimental curves well (Figure 2B–D). During fitting of the equation  $Z_{DL} = C_{DL}^{\prime-1} \cdot (j\omega)^{-n}$  for the CPE, the exponent n consistently remained above 0.9, indicating that the parameter  $C_{DL}^{\prime}$  is very close to the actual EDL capacitance (Figure 2E). Additionally, minimal capacitances  $C_{DL, min}^{\prime}$  can be observed for all Pt(hkl) surfaces (Figure 2A), for which the exponent approaches to 1.

Surface coordination, particularly generalized coordination numbers  $^{22,24}$  (see Supporting Information, Section 1), enables a useful parametrization of the surfaces simultaneously in energetic and structural terms. In other words, one can use GCNs to characterize and quantify the affinity of the surface for electrolyte components. In Figure 3, the  $C'_{DL, min}$  values extracted from Figure 2A are plotted versus the special parameter explained as follows (see the description for this parameter and its meaning in the SI, Figure S1, and ref 17). Consider that the GCN can be understood as a measure of "nonsaturated electron density" at the surface. It is possible to hypothesize that the higher the GCN, the lower the densities and the longer the effective distances between the surface atoms and the first water layer. Therefore, it is reasonable to

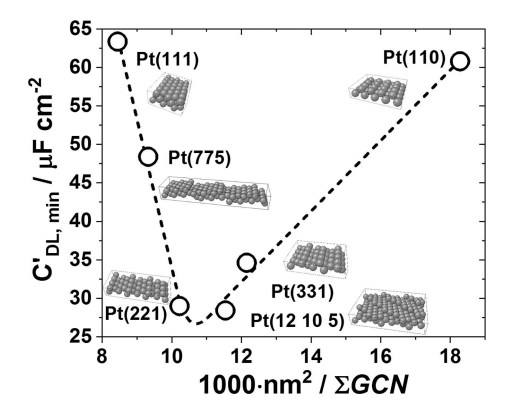


**Figure 3.** Minimal double layer capacitances as a function of the  $F_{\rm e}$  parameter (expressed as  $1000 \cdot {\rm nm^2/\Sigma GCN})^{17}$  for the Pt(hkl) electrodes.

define a new function,  $F_e$ , which should be connected to the  $C'_{DL, min}$  values in a first approximation:<sup>17</sup>

$$F_{\rm e} = \text{Unit Surface Area} / \sum \text{GCN}$$

One can see from Figure 3 that for the Pt(hkl) electrodes, a (inverse) volcano-type relationship can be observed. Namely, the  $C'_{DL,\ min}$  values decrease linearly as the  $F_{\rm e}$  parameter (expressed as  $1000\cdot {\rm nm}^2/\Sigma {\rm GCN}$  in Figure 3) increases, ranging from Pt(111), Pt(775) to Pt(221), but the values then increase linearly with the increase in  $F_{\rm e}$  parameter, ranging from Pt(12 10 5), Pt(331) to Pt(110). This relationship shows the strong dependence of the EDL capacitance of the Pt single-crystal electrodes on the surface structure. The maximum value of  $\sim 60\ \mu{\rm F}\cdot{\rm cm}^{-2}$  for Pt(111) and Pt(110) is over twice as large as the minimum value of  $\sim 28\ \mu{\rm F}\cdot{\rm cm}^{-2}$  for Pt(221) and Pt(12 10 5) (Figure 3). This significant difference suggests that the EDL structure can vary based on the different surface structures.

To explain the results of the electrochemical measurements of the EDL capacitance, we performed AIMD simulations of Pt/water interfaces (see the corresponding atomic structures in Figure S3). Here, we chose four representative Pt facets, Pt(111), Pt(221), Pt(331), and Pt(110), for our simulations, which should cover the whole interval of the measured EDL capacitances. Figure 4 shows the evaluated dipole angle ( $\psi$ ) distributions and OH angle ( $\theta$ ) distributions for each Pt/water interface. The distributions and average dipole moments calculated separately for the first and second water layers are given in the SI. The angles depicted in the figure are taken with respect to the surface normal, i.e., along the positive z-direction.  $\psi$  corresponds to the angle between the dipole

moment direction of each water molecule and the surface normal, and  $\theta$  represents the angle between each O–H bond and the surface normal. Thus,  $\psi=90^\circ$  along with  $\theta=90^\circ$  represents a water molecule that lays "flat" on the slab surface. Angles between  $0^\circ$  and  $90^\circ$  indicate that water is oriented in an H-up configuration, and angles between  $90^\circ$  and  $180^\circ$  indicate that water orientation is H-down.

It is seen from the left plot of Figure 4 that the dipole angles  $(\psi)$  for all facets have a larger distribution above  $90^{\circ}$  in the overall EDL, indicating a more H-down orientation of water molecules. This is confirmed by the average dipole angles shown in Figures S7 and the average of  $\cos(\psi)$  shown in Figure 5. The (221) and (331) facets prefer the H-down

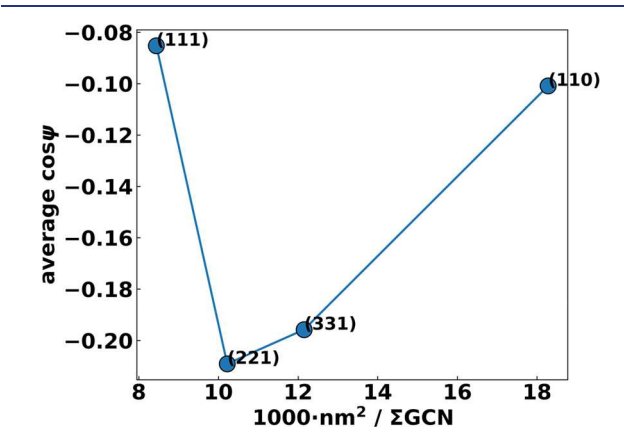


Figure 5. Average  $\cos(\psi)$  at EDL vs the  $F_{\rm e}$  parameter (represented as  $1000 \cdot {\rm nm^2/\Sigma GCN}$ ) at Pt/water interfaces derived from AIMD simulations.

orientation more strongly than the (111) and (110) facets, as seen by the lower magnitude of peaks in the  $0^{\circ}-90^{\circ}$  region in Figure 4, as well as the more negative value of average  $\cos(\psi)$  in Figure 5. This is due to the effect of H-up chemisorbed water on step sites, which orients the water on the terrace region in the H-down direction. The distance between steps at (221) is greater than that at (331), which enables more H-down water molecules, as shown in Figure 6b. This orientation effect is absent in the (111) and (110) facets. The  $\theta$  distributions (right plot in Figure 4) contain a peak close to  $70^{\circ}-90^{\circ}$  and another close to  $160^{\circ}$ . These peaks are more well-defined in (111) and (110) compared to (221) and (331) due to different orientations of waters on step and terrace sites for the latter facets. The low distributions of the O–H angles

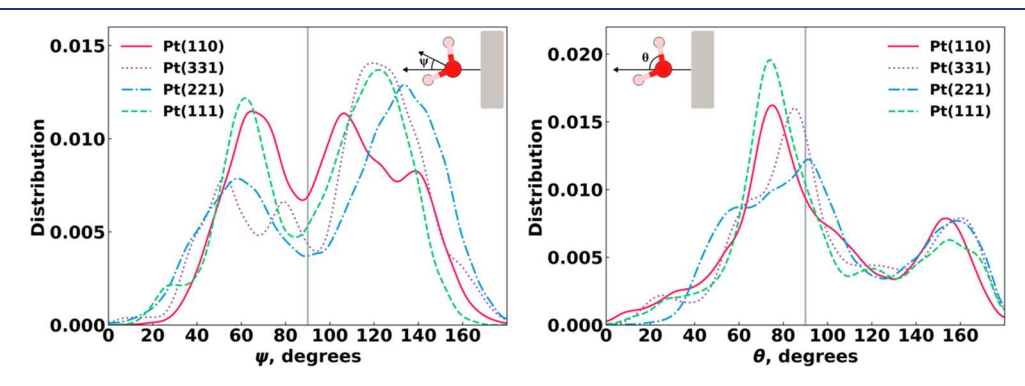


Figure 4. Dipole angle  $(\psi)$  distribution and OH angle  $(\theta)$  distribution at Pt/water interfaces were derived from AIMD simulations.

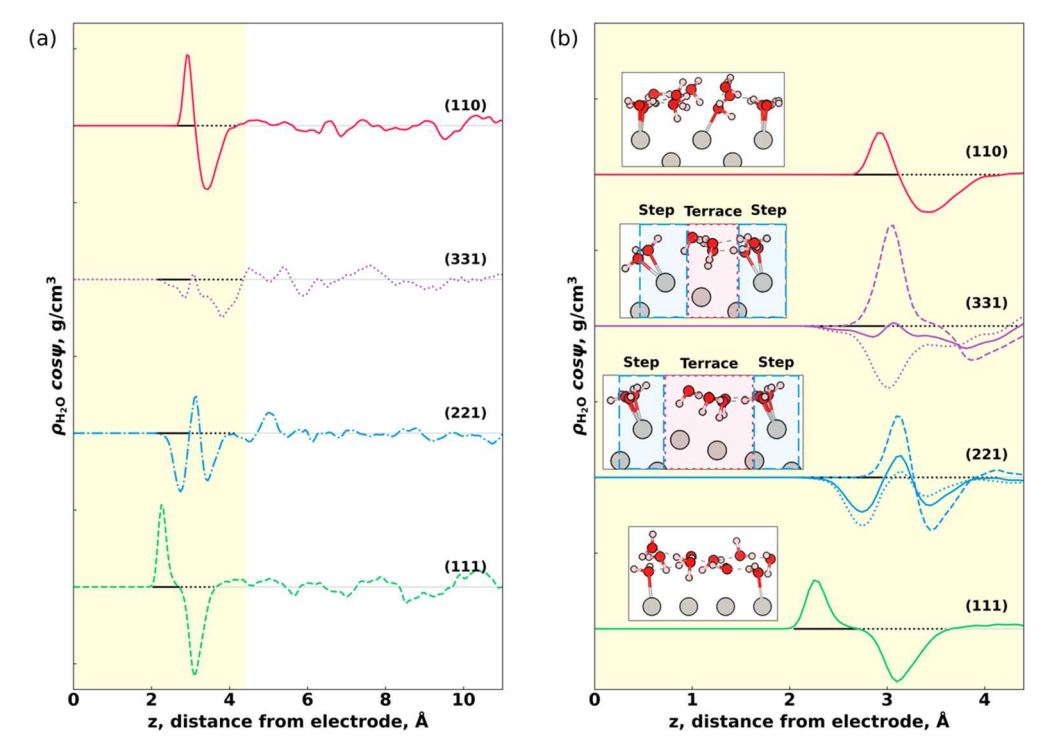


Figure 6. (a) Distribution profiles of the mean dipole orientation of water ( $\rho_{\rm H2O}$  cos  $\psi$ ) for different Pt/water interfaces. (b) Splitting of the distributions for the major interfacial region (shown as a yellow background) between water molecules over the step and terrace sites. Horizontal solid and dotted black lines in both (a) and (b) indicate the interfacial regions corresponding to the EDL's first and second water layers, respectively.

 $(\theta)$  at smaller angles and the peak close to 160° support that H-down orientations are preferred over H-up.

We next analyze the distribution of dipole orientations ( $\rho_{\rm H2O}$  $\cos \psi$ ) with respect to the distance from interfaces (see Figure 6). A positive value of  $cos(\psi)$  indicates the H-up orientation, and negative values indicate the H-down orientation. Horizontal solid black lines indicate the first water layers of the EDL for different facets, and the second water layers are indicated by dotted black lines. It can be observed that moving from the interface to the bulk region, the (111) and (110) facets feature a positive peak at ~2 Å, indicating a distribution of H-up-oriented water. On the other hand, the (221) and (331) facets feature a negative peak indicating a distribution of H-down oriented water. The second water layer at ~3 Å in (111) and (110) shows only H-down orientations, while in (221) and (331), there is a small positive peak followed by a negative peak. In Figure 6b, the (221) and (331) distributions are further split into distributions over step and terrace sites, as illustrated in the insets. The initial negative peak for these facets is found to occur from H-down water orientations over the terrace sites. Figure 5 shows the average cosine of dipole moment angles at the EDL at the Pt/water interfaces vs the  $F_{\rm e}$ parameter (represented as  $1000 \cdot \text{nm}^2/\Sigma GCN$ ), similar to the representation of the measured EDL capacitances (see Figure 3). The values of  $cos(\psi)$  follow the trend expected from Figures 4 and 6, i.e., with water molecules at the (221) and (331) surfaces being more strongly oriented in the H-down direction. This trend is similar to the experimental data presented in Figure 3.

Our computational results qualitatively agree with the recent data obtained for the Pt(111)/water interface employing constant Fermi-level AIMD simulations.<sup>32</sup> In particular, it was found that the interfacial water molecules exhibit a slight

preference for the H-down configurations at the PZC, consistent with our dipole orientation analysis (Figure 5). The double layer capacitance was estimated to be low under negative bias when most interfacial water molecules are found in H-down configurations, reaching much higher values upon increasing the potential to cause water dipole reorientation to H-up configurations. The observed main peak in the  $C'_{DL, min}$  at  $U=0.33~\rm V_{SHE}$  was associated with the atomic structure reorganization of the water double layer. Our results also indicate much higher measured EDL capacitances for the (111) and (110) facets than for (221) and (331) that feature much stronger H-down water orientations (Figure 5).

In another recent AIMD-based investigation, a series of stepped Pt/water interfaces at the PZC was examined.<sup>33</sup> It was found that the step density significantly influences the atomic structures of the Pt/water interfaces. In particular, it was determined that the step sites of metal surfaces are preferred more for water chemisorption than the terrace sites, in overall agreement with our findings. In the same study, it was shown that the PZC changes roughly linearly with increasing step density. According to these theoretical estimates, the difference in PZC between Pt facets with comparable step densities (such as Pt(111) and Pt(221) in our work) turned out to be less than 0.2 V. It was found that the higher the step density, the lower the PZC. Importantly, it was determined that the computationally predicted value of the EDL capacitance for Pt(111) of about 0.22  $V_{SHE}$  agrees well with reported experimental data of 0.28–0.37  $V_{SHE}$ . Given these theoretical insights, our computational estimates of the capacitance between the two sets of surfaces, Pt(111) and Pt(110), and Pt(221) and Pt(331), obtained under the PZC conditions should be consistent with the capacitance data presented in Figure 2

even though the capacitance strongly depends on the electrode potential.

To provide further insights into the interfacial water structure and to rationalize the volcano-like shape of the EDL capacitance vs the  $F_{e^-}$  parameter observed experimentally (see Figure 3), we propose the following explanation based on our present AIMD simulations. Specifically, when the step density increases from 0 nm<sup>-1</sup> for Pt(111) to 1.19 nm<sup>-1</sup> for Pt(221) and 1.63 nm<sup>-1</sup> for Pt(331), water molecules that prefer to chemisorb on the step sites in H-up configurations make the motion of nearby water species also more rigid through the H-bonding network. This is indicated by the prominent negative peaks for both Pt(221) and Pt(331) at about 3 Å in Figure 6b that correspond to H-down water orientations over the terrace sites. This rigidity is also reflected in much lower average dipole moments for (221) and (331) in Figure 5, resulting in a decrease in the double layer capacitance. However, with a further increase in the step density, such as in the case of 2.51 nm<sup>-1</sup> for Pt (110), disruption of the water structure due to chemisorbed water at the interface becomes more pronounced, leading to an overall softening of the water structure, higher average dipole moment, and thus an increased EDL capacitance. Overall, our theoretical insights into the atomic-scale structure of the EDL allow us to rationalize the volcano shape of the EDL capacitance as a function of the step density derived from electrochemical measurements.

## CONCLUSIONS

In this work, by employing electrochemical impedance spectroscopy measurements, we have demonstrated a strong dependence of the EDL capacitance of the Pt single-crystal electrodes in acidic media on the electrode structure, resulting in more than twice larger values for the Pt(111) and Pt(110) surfaces than for Pt(221) and Pt(12 10 5). Additional ab initio molecular dynamics simulations helped to explain the experimental observations by structural reorganization of the water double layer. In particular, computational results reveal different dipole moment orientations of water molecules at the interface depending on the electrode structure, showing a much stronger preference for H-down configurations at (221) and (331) than at (111) and (110) surfaces of Pt at the potential of zero charge. We believe that our electrochemical investigation of the well-characterized Pt surfaces is an important step toward a deeper understanding of the influence of the electrode atomic structure on the basic electrochemical properties of electrocatalytic materials.

#### ASSOCIATED CONTENT

## Supporting Information

The Supporting Information is available free of charge at https://pubs.acs.org/doi/10.1021/jacs.3c11403.

Additional details and supporting figures for experimental and computational parts of this study. (PDF)

## AUTHOR INFORMATION

## **Corresponding Authors**

Vitaly Alexandrov — Department of Chemical and Biomolecular Engineering and Nebraska Center for Materials and Nanoscience, University of Nebraska—Lincoln, Lincoln, Nebraska 68588, United States; orcid.org/0000-0003-2063-6914; Email: valexandrov2@unl.edu Aliaksandr S. Bandarenka — Physics of Energy Conversion and Storage, Department of Physics, Technical University of Munich, 85748 Garching bei München, Germany; Catalysis Research Center, Technical University of Munich, 85748 Garching bei München, Germany; orcid.org/0000-0002-5970-4315; Email: bandarenka@ph.tum.de

#### **Authors**

Song Xue – Physics of Energy Conversion and Storage, Department of Physics, Technical University of Munich, 85748 Garching bei München, Germany; Advanced Chemical Engineering and Energy Materials Research Center, China University of Petroleum (East China), Qingdao 266580, China

Payal Chaudhary — Department of Chemical and Biomolecular Engineering and Nebraska Center for Materials and Nanoscience, University of Nebraska—Lincoln, Lincoln, Nebraska 68588, United States; Orcid.org/0000-0002-8863-5646

Mohammad Reza Nouri — Department of Chemical and Biomolecular Engineering and Nebraska Center for Materials and Nanoscience, University of Nebraska—Lincoln, Lincoln, Nebraska 68588, United States; orcid.org/0000-0002-6046-200X

Elena Gubanova — Physics of Energy Conversion and Storage, Department of Physics, Technical University of Munich, 85748 Garching bei München, Germany; orcid.org/0000-0003-3375-9833

Batyr Garlyyev – Physics of Energy Conversion and Storage, Department of Physics, Technical University of Munich, 85748 Garching bei München, Germany; orcid.org/0000-0002-2756-2105

Complete contact information is available at: https://pubs.acs.org/10.1021/jacs.3c11403

# **Author Contributions**

\*S.X. and P.C. contributed equally.

## Notes

The authors declare no competing financial interest.

#### ACKNOWLEDGMENTS

We thank the German Research Foundation (DFG) under Germany's excellence strategy — EXC 2089/1 — 390776260, Germany's excellence cluster "e-conversion" and TUM IGSSE, Project 14.06. V.A. acknowledges the National Science Foundation (NSF) support through the NSF CAREER award (Grant No. CBET-1941204). This work used the Expanse cluster at the San Diego Supercomputer Center at UC San Diego through allocation CHE230023 from the Advanced Cyberinfrastructure Coordination Ecosystem: Services & Support (ACCESS) program, which is supported by National Science Foundation grants #2138259, #2138286, #2138307, #2137603, and #2138296.

## **■** REFERENCES

- (1) Grahame, D. C. Differential capacity of mercury in aqueous sodium fluoride solutions. I. Effect of concentration at 25°. *J. Am. Chem. Soc.* **1954**, *76*, 4819–4823.
- (2) Grahame, D. C. The electrical double layer and the theory of electrocapillarity. *Chem. Rev.* **1947**, *41*, 441–501.
- (3) Lust, E. Electrical double layers. Double layers at single-crystal and polycrystalline electrodes. *Encyclopedia of Electrochemistry*; Bard, A. J., Eds.; Wiley: 2002. DOI: 10.1002/9783527610426.bard010204

- (4) Ojha, K.; Doblhoff-Dier, K.; Koper, M. T. M. Double-layer structure of the Pt(111)-aqueous electrolyte interface. *Proc. Nat. Academy of Sci. USA* **2022**, *119*, e2116016119.
- (5) Ojha, K.; Arulmozhi, N.; Aranzales, D.; Koper, M. T. M. Double layer at the Pt(111)-aqueous electrolyte interface: Potential of zero charge and anomalous Gouy-Chapman screening. *Angew. Chem., Int. Ed.* **2020**, *59*, 711–715.
- (6) Sakong, S.; Groß, A. The electric double layer at metal-water interfaces revisited based on a charge polarization scheme. *J. Chem. Phys.* **2018**, *149*, No. 084705.
- (7) Skúlason, E.; Karlberg, G. S.; Rossmeisl, J.; Bligaard, T.; Greeley, J.; Jónsson, H.; Nørskov, J. K. Density functional theory calculations for the hydrogen evolution reaction in an electrochemical double layer on the Pt(111) electrode. *Phys. Chem. Chem. Phys.* **2007**, *9*, 3241.
- (8) Schmickler, W. The effect of weak adsorption on the double layer capacitance. *ChemElectroChem.* **2021**, *8*, 4158.
- (9) Magnussen, O. M.; Groß, A. Toward an atomic-scale understanding of electrochemical interface structure and dynamics. *J. Am. Chem. Soc.* **2019**, *141*, 4777–4790.
- (10) Huang, J.; Malek, A.; Zhang, J.; Eikerling, M. H. Non-monotonic surface charging behavior of platinum: a paradigm change. *J. Phys. Chem. C* **2016**, 120, 13587.
- (11) Doblhoff-Dier, K.; Koper, M. T. M. Modeling the Gouy-Chapman diffuse capacitance with attractive ion—surface interaction. *J. Phys. Chem. C* **2021**, *125*, 16664–16673.
- (12) Simon, P.; Gogotsi, Y.; Dunn, B. Where do batteries end and supercapacitors begin? *Science* **2014**, *343*, 1210–1211.
- (13) Sebastián-Pascual, P.; Shao-Horn, Y.; Escudero-Escribano, M. Toward understanding the role of the electric double layer structure and electrolyte effects on well-defined interfaces for electrocatalysis. *Curr. Opin. Electrochem.* **2022**, 32, 100918.
- (14) Monteiro, M. C. O.; Goyal, A.; Moerland, P.; Koper, M. T. M. Understanding cation trends for hydrogen evolution on platinum and gold electrodes in alkaline media. *ACS Catal.* **2021**, *11*, 14328–14335.
- (15) Colic, V.; Pohl, M.; Scieszka, D.; Bandarenka, A. S. Influence of the electrolyte composition on the activity and selectivity of electrocatalytic centers. *Catal. Today* **2016**, *2*62, 24–35.
- (16) Huang, B.; Rao, R. R.; You, S.; Myint, K. H.; Song, Y.; Wang, Y.; Ding, W.; Giordano, L.; Zhang, Y.; Wang, T.; Muy, S.; Katayama, Y.; Grossman, J. C.; Willard, A. P.; Xu, K.; Jiang, Y.; Shao-Horn, Y. Cation- and pH-dependent hydrogen evolution and oxidation reaction kinetics. J. Am. Chem. Soc. Au. 2021, 10, 1674–1687.
- (17) Gubanova, E.; Schmidt, T. O.; Watzele, S.; Alexandrov, V.; Bandarenka, A. S. Structure-dependent electrical double layer capacitances of the basal plane Pd(hkl) electrodes in HClO<sub>4</sub>. *J. Phys. Chem. C* **2022**, *126*, 11414–11420.
- (18) Garlyyev, B.; Xue, S.; Watzele, S.; Scieszka, D.; Bandarenka, A. S. Influence of the nature of the alkali metal cations on the electrical double-layer capacitance of model Pt(111) and Au(111) electrodes. *J. Phys. Chem. Lett.* **2018**, *9*, 1927–1930.
- (19) Xue, S.; Garlyyev, B.; Auer, A.; Kunze-Liebhäuser, J.; Bandarenka, A. S. How the nature of the alkali metal cations influences the double-layer capacitance of Cu, Au and Pt single-crystal electrodes. *J. Phys. Chem. C* **2020**, *124*, 12442–12447.
- (20) Martynov, G. A.; Salem, R. R. The electronic capacitor at a metal-electrolyte interface. *Can. J. Chem.* 1984, 62, 1145–1158.
- (21) Emets, V. V.; Damaskin, B. B. Comparative study of the electrical double layer on liquid electrodes of mercury, gallium, and an In-Ga alloy in hexamethylphosphortriamide. *Russ. J. Electrochem.* **2006**, 42, 789–797.
- (22) Calle-Vallejo, F.; Tymoczko, J.; Colic, V.; Vu, Q. H.; Pohl, M. D.; Morgenstern, K.; Loffreda, D.; Sautet, P.; Schuhmann, W.; Bandarenka, A. S. Finding optimal surface sites on heterogeneous catalysts by counting nearest neighbors. *Science* **2015**, *350*, 350.
- (23) Bandarenka, A. S. Development of hybrid algorithms for EIS data fitting. In *Lecture notes on impedance spectroscopy. Measurement, modeling and applications*, Vol. 4; Kanoun, O., Ed.; CRC Press, Tailor and Francis Group: London, 2013; pp 29–36.

- (24) Calle-Vallejo, F.; Bandarenka, A. S. Enabling generalized coordination numbers to describe strain effects. *ChemSusChem* **2018**, *11*, 1824–1828.
- (25) Calle-Vallejo, F. The ABC of generalized coordination numbers and their use as a descriptor in electrocatalysis. *Adv. Sci.* **2023**, *10*, 2207644.
- (26) Kühne, T. D.; Iannuzzi, M.; Del Ben, M.; Rybkin, V. V.; Seewald, P.; Stein, F.; et al. CP2K: an electronic structure and molecular dynamics software package quickstep: efficient and accurate electronic structure calculations. *J. Chem. Phys.* **2020**, *152*, 194103
- (27) Goedecker, S.; Teter, M.; Hutter, J. Separable dual-space gaussian pseudopotentials. *Phys. Rev. B* **1996**, *54*, 1703–1710.
- (28) Perdew, J. P.; Burke, K.; Ernzerhof, M. Generalized gradient approximation made simple. *Phys. Rev. Lett.* **1996**, *77*, 3865–3868.
- (29) Grimme, S.; Antony, J.; Ehrlich, S.; Krieg, H. A consistent and accurate ab initio parametrization of density functional dispersion correction (DFT-D) for the 94 elements H-Pu. *J. Chem. Phys.* **2010**, 132, 154104.
- (30) Grimme, S.; Ehrlich, S.; Goerigk, L. Effect of the damping function in dispersion corrected density functional theory. *J. Comput. Chem.* **2011**, 32, 1456.
- (31) van der Niet, M. J. T. C.; Garcia-Araez, N.; Hernández, J.; Feliu, J. M.; Koper, M. T. M. Water dissociation on well-defined platinum surfaces: The electrochemical perspective. *Catal. Today* **2013**, 202, 105.
- (32) Bouzid, A.; Pasquarello, A. Atomic-scale simulation of electrochemical processes at electrode/water interfaces under referenced bias potential. *J. Phys. Chem. Lett.* **2018**, *9*, 1880–1884.
- (33) Chen, A.; Le, J. B.; Kuang, Y.; Cheng, J. Modeling stepped Pt/water interfaces at potential of zero charge with ab initio molecular dynamics. *J. Chem. Phys.* **2022**, *157*, No. 094702.
- (34) Pajkossy, T.; Kolb, D. M. Double layer capacitance of Pt(111) single crystal electrodes. *Electrochemica Acta* **2001**, *46*, 3063–3071.